# Performance Evaluation of a Low-Complexity Receiver Concept for TOA-Based Ultrawideband Ranging

Giovanni Bellusci, Gerard J. M. Janssen, Junlin Yan, and Christian C. J. M. Tiberius

***Abstract*—In this paper, a novel low-complexity time-of-arrival (TOA) estimation strategy and a conceptual receiver setup for ultrawideband (UWB) signals is proposed, and its performance is evaluated. The receiver consists of an analog peak detector followed by two *RC* filters with different time constants. From two exponentially decaying signals, the TOA of the first peak of the received signal is reconstructed. This solution requires simple signal processing and sampling rates on the order of only a few tens of megahertz. At the same time, the achieved range error is at centimeter level since the large signal bandwidth used is fully exploited. To allow for performance flexibility, a statistical framework is proposed in which results of multiple initial TOA estimates are combined into a final estimate. Impairments due to narrowband interference are investigated, and a coarse acquisition scheme based on maximum energy detection is described. This last step is required for proper operation of the TOA receiver. A link budget analysis, which is based on the FCC power limitations for UWB signals, shows that reliable ranging is feasible up to 300 m in line-of-sight situations and up to 60 m in non-line-of-sight cases. The presented solution avoids the main technological challenges, namely extremely high sampling rates and complex processing at the receiver, which currently limit practical implementations of high-precision UWB positioning systems.**

***Index Terms*—Ranging, time-of-arrival (TOA) estimation, ultrawideband (UWB).**

## I. Introduction

RECENTLY, indoor positioning has been attracting considerable attention from both research and industry. Logistics, healthcare applications, search and rescue, military services, and tracking of objects and people are a few examples of applications that can benefit from having precise localization information. However, in indoor environments, traditional satellite-based positioning services such as GPS are usually unavailable, unreliable, or inaccurate. Therefore, alternative solutions need to be developed.

Manuscript received July 18, 2011; revised March 6, 2012; accepted June 9, 2012. Date of publication July 10, 2012; date of current version November 6, 2012. This work was supported by the Technology Foundation STW. The review of this paper was coordinated by Prof. R. C. Qiu.

G. Bellusci is with Xsens Technologies B.V., 7521 PR Enschede, The Netherlands (e-mail: giovanni.bellusci@xsens.com).

G. J. M. Janssen is with the Faculty of Electrical Engineering, Mathematics and Computer Sciences, Delft University of Technology, 2628 CD Delft, The Netherlands (e-mail: G.J.M.Janssen@tudelft.nl).

J. Yan is with Intel Mobile Communications GmbH, 47259 Duisburg, Germany (e-mail: junlin.yan@intel.com).

C. C. J. M. Tiberius is with the Faculty of Civil Engineering and Geosciences, Delft University of Technology, 2628 CN Delft, The Netherlands (e-mail: C.C.J.M.Tiberius@tudelft.nl).

Digital Object Identifier 10.1109/TVT.2012.2207749

A common way to perform positioning is based on time-of-arrival (TOA) estimation. From the signal travel time, the distance between transmitter and receiver can be calculated; this is the basic operation for range-based positioning [4]. Ultrawideband (UWB) technology [1], [2] has been identified as a promising candidate to provide highly accurate positioning information in indoor environments in which radio propagation takes place via hundreds of different paths [3] closely separated in time. The use of subnanosecond UWB pulse signals allows for distinguishing the different multipath components and for accurately estimating the TOA of the *first* path, which contains the relevant information for ranging. With UWB signals, centimeter-level positioning accuracy can be achieved, even in indoor multipath-rich environments [4]–[9].

Using UWB pulse signals in practical systems introduces significant challenges in the processing of gigahertz bandwidth waveforms at the receiver side. Most of the proposed solutions in literature rely on samples of the received signal collected at least at the Nyquist rate [7]–[9]. For example, a sampling rate of 20.5 GHz is used for the generalized maximum-likelihood TOA estimator proposed in [9]. However, the extremely fast analog-to-digital converters (ADCs) required and the high hardware demands for processing, currently prevent the use of UWB positioning technology for a wide range of applications with mass-market potential since they typically have strict requirements on cost, complexity, and power consumption.

To address this issue, suboptimal and lower complexity approaches have been investigated, in which part of the potential accuracy is sacrificed. In [10], an energy-based TOA estimation is proposed where the accuracy depends on the sampling rate used, e.g., it is at meter level using a 500-MHz ADC. A conceptually similar approach is proposed in [11] where the time window in which the received signal is observed is divided in small time bins; the center of the first bin whose energy exceeds a given threshold is detected as the signal TOA. This last solution, while attractive since it avoids the need for high sampling rates, presents the following drawbacks: 1) its TOA estimation accuracy is particularly sensitive to noise and interference since the approach is based on bin energy detection; and 2) the potential centimeter accuracy provided by UWB technology is not fully exploited since the performance is limited by the bin size, typically of a few nanoseconds, resulting in a decimeter-to-meter additional bin quantization error.

In this paper, a novel low-complexity TOA estimation technique is proposed based on the following considerations. For short-duration UWB pulses, the received signal is an approximation of the channel impulse response (CIR) with a time resolution given by the inverse of the signal bandwidth. The proposed receiver consists of an analog peak detector operating directly on the received signal, which is followed by two $RC$ filters with different time constants (as shown in Fig. 2). From the two differently exponentially decaying signals, which are sampled at a low rate, the first-peak TOA is calculated. It is shown that very simple signal processing and a sampling rate of only a few tens of megahertz are needed, i.e., about two orders of magnitude less than the Nyquist rate. The sources of error specifically introduced by the proposed receiver concept are shown to be negligible. Therefore, the accuracy of the proposed approach is practically the same as of an ideal first-peak detector based on the Nyquist sampling and perfect reconstruction of the received signal envelope, resulting in a range error at centimeter level. This receiver can also work in a time-difference-of-arrival (TDOA) setup, i.e., the receiver clock does not need to be synchronized with the transmitter clocks. The receiver clock offset is then estimated in the positioning algorithm.

Because the proposed receiver directly estimates the TOA from the instantaneous received pulse signal without further processing, it is not possible to increase the effective SNR by performing an average *before* TOA estimation. To allow for flexibility in performance and reliability, a statistical processing framework is proposed to enhance the range accuracy by combining multiple TOA estimates. Using this framework, the effect of narrowband interference (NBI) is analyzed based on the first threshold crossing probability evaluated for Gaussian processes and time-varying boundaries [17], [18]. To the best of the authors' knowledge, previous literature has only focused on communications applications [12]–[15] or bin-energy-based TOA estimation [16], whereas no results are available for NBI impairments on peak-detection-based TOA estimation techniques. A coarse acquisition scheme [19]–[21], required for correct operation of the proposed TOA estimation strategy, is next described. To keep system complexity low, coarse acquisition is based on energy detection. The presented theoretical framework to calculate the statistics of the maximum energy time window in closed form allows evaluation of the performance of the scheme in terms of probability of acquisition and to relate this to the relevant system and channel parameters, which is another novelty of this paper. Finally, the coverage area for reliable ranging using the proposed techniques is determined based on the FCC power limitations for UWB signals using a link budget analysis for line-of-sight (LOS) and non-line-of-sight (NLOS) cases.

This paper is organized as follows. Section II introduces the system model. In Section III, the low-complexity receiver concept for TOA estimation is introduced and its performance analyzed. Section IV investigates the impairments on the proposed approach due to NBI. In Section V, the coarse acquisition scheme is analyzed, and Section VI provides a link budget analysis to determine the maximum coverage of the proposed solution. Finally, in Section VII, concluding remarks are given.

## II. Signal Model

The received UWB pulse signal in a multipath channel can be represented as

$$r(t) = \sum_{j=-\infty}^{\infty} c_j w_{\mathrm{mp}}(t - jT_f) + n(t) \tag{1}$$

where $c_j \in \{\pm 1\}$ is a random polarity code used to avoid peaks in the power spectral density of the received signal, $T_f$ is the frame repetition period, and $n(t)$ is the additive white Gaussian noise with zero-mean and single-sided power spectral density $N_0$. The received multipath signal $w_{\mathrm{mp}}(t)$ results from the transmission of a single pulse $w(t)$ with energy $E_w$, and it is expressed as

$$w_{\mathrm{mp}}(t) = \sum_{l=0}^{L_{\mathrm{ch}}-1} h_l w_l(t - \tau_l) \tag{2}$$

where $h_l$ and $\tau_l$ are the amplitude coefficient and the delay of the $l$th multipath component, respectively; $w_l(t)$ is the waveform received along the $l$th path; and $L_{\mathrm{ch}}$ is the number of multipath components. This is a general indoor multipath propagation model in which each single path may suffer distortion. The unknown TOA of the received signal is indicated as $\tau_0$. Without loss of generality, we can assume $\tau_0 \in [0, T_f]$ since we are interested in the TOA with respect to the receiver clock. The absolute value of $\tau_0$ needs to be determined with higher layer protocols (e.g., two-way ranging) or with a TDOA scheme.

In the analysis and simulation results presented in the following, $w(t)$ is chosen as a Gaussian-pulse-modulated carrier, i.e.,

$$w(t) = A_0 \cos(2\pi f_0 t) \exp\left(-t^2 / \left(2T_g^2\right)\right) \tag{3}$$

where $A_0$ is a normalization factor, $f_0 = 4.6$ GHz is the central frequency of the spectrum, and $T_g = 0.16$ ns, which corresponds to a $-10$ dB bandwidth $B$ of 3 GHz between 3.1 and 6.1 GHz. An additional bandpass filter is used to further cut off emissions outside the specified bandwidth and to satisfy the FCC mask imposed for UWB transmissions [22]. The results presented in the following, however, are general and can also be applied to a different pulse shape.

## III. Time-of-Arrival Estimation

A low-complexity receiver concept is proposed for accurate TOA estimation of the first peak of the received signal, and the sources of inaccuracy introduced by this setup are analyzed. To improve signal quality and to allow for a tradeoff between performance and measurement latency, a strategy to combine multiple TOA estimates is described and evaluated.

It is assumed that an estimate $T_0$ of the frame starting time, e.g., provided by a preliminary coarse acquisition step, as discussed in Section V, is available. Now, the TOA of the received signal $\tau_0$ can be expressed as $\tau_0 = T_0 + \tau$. Here, we will focus on the estimation of $\tau$. To avoid detection of late multipath components belonging to the tail of a previous frame, it is required that $0 \le \tau \le T_f - \tau_{\mathrm{cds}}$, where $\tau_{\mathrm{cds}}$ is the delay

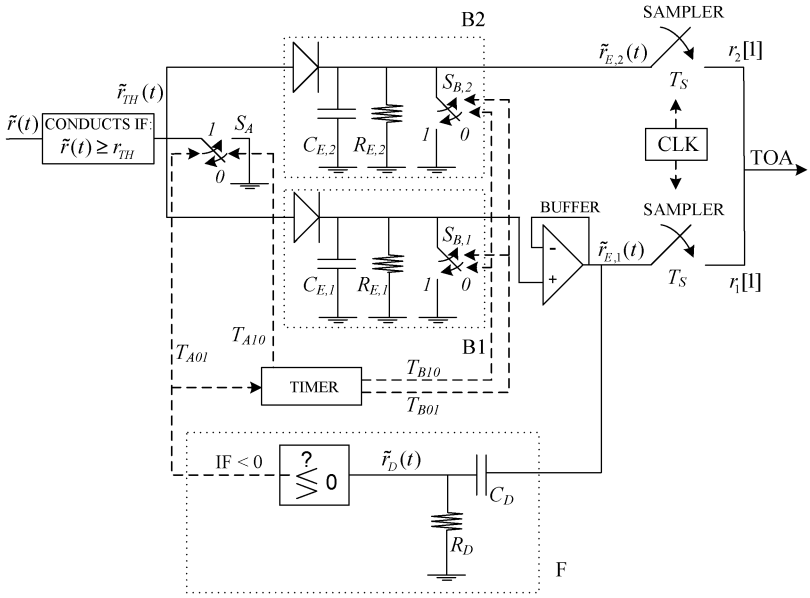


Fig. 1. Proposed low-complexity receiver to estimate the TOA of the received signal.

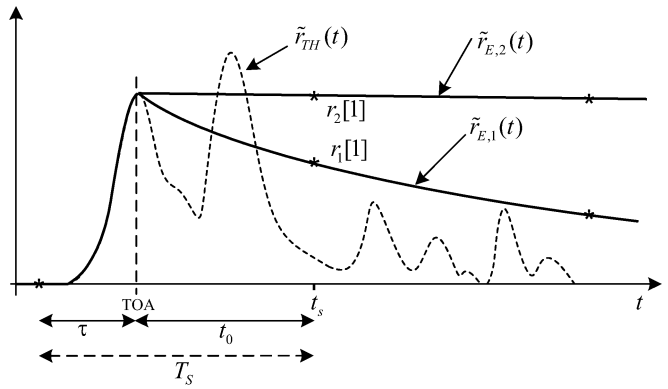


Fig. 2. Principle of working of the proposed receiver.

spread of the channel. This is equivalent to the requirement that the received signal in the observed window starts with a noise-only part of duration $\tau$, followed by the useful signal part (of duration $\tau_{\rm cds}$), which goes to zero before the end of the frame.

### A. Receiver Concept

The proposed receiver for TOA estimation, with a principle of implementation as depicted in Fig. 1, exploits the fact that the received signal can be considered a good approximation of the CIR when short-duration UWB pulses are used. The received signal is directly passed through two analog processing branches consisting of a peak detector followed by an $RC$ circuit with a different time constant per branch, which cause an exponential decrease in the output signal with time from the detected first-path amplitude. In the following, we will assume an *ideal* peak detector in our analysis. The outputs of both branches are sampled with a relatively low sampling rate, as shown in Fig. 2, which illustrates the principle of operation of the described receiver. From the collected samples, it is possible to accurately retrieve the TOA of the first path. In the following, the principle of operation of this receiver is described.

Referring to Fig. 1, the received signal $r(t)$ is passed through a filter matched to the transmitted pulse $w(t)$ for noise reduction and to simplify the theoretical analysis. In practice, a bandpass filter can be used at the cost of a small performance degradation (a fraction of a decibel). The envelope $\tilde{r}(t)$ of the filter output is determined and goes to a threshold device with an input–output relation given by

$$\tilde{r}_{\rm TH}(t) = \begin{cases} \tilde{r}(t), & \text{if } \tilde{r}(t) \geq r_{\rm TH} \\ 0, & \text{otherwise} \end{cases} \tag{4}$$

which cuts off noise and signal components smaller than $r_{\rm TH}$. The default position of the switches $S_A$, $S_{B,1}$, and $S_{B,2}$ is "0" (open circuit). The signal $\tilde{r}_{\rm TH}(t)$ is fed to the blocks $B1$ and $B2$. Block $B1$, consists of a peak detector composed of a diode followed by an $RC$ circuit. The values of $R_{E,1}$ and $C_{E,1}$ are set to affect the output signal with the "diagonal clipping" phenomenon [23]; the time constant of the circuit $\tau_{E,1} = R_{E,1}C_{E,1}$ in fact is chosen larger than the inverse of the signal bandwidth. In this way, the output, instead of following the envelope of the signal, tends to exponentially decrease with time from the detected peak value. Block $B2$ works in the same way, however, with a different time constant. Output $\tilde{r}_{E,1}(t)$ of $B1$ is used by block $F$ that contains a trigger circuit to detect a sudden positive change of its value, which results in a trigger to control switches $S_A$, $S_{B,1}$, and $S_{B,2}$. The buffer amplifier between blocks $B1$ and $F$ prevents the circuits from loading each other. The trigger circuit consists of an $RC$ differentiator to derive a trigger signal when $\tilde{r}_D(t)$ goes from positive to negative. To work properly, its time constant $\tau_D = R_D C_D$ should be less than $1/B$. When a trigger occurs due to a first peak of the signal envelope, $S_A$ is switched to the short-circuit position at time $T_{A_{01}}$ to prevent detection of later peaks, and a timer is set to control switches $S_{B,1}$ and $S_{B,2}$ with a specified delay. After a trigger occurred, $\tilde{r}_{\rm TH}(t)$ does not influence $\tilde{r}_{E,1}(t)$ and

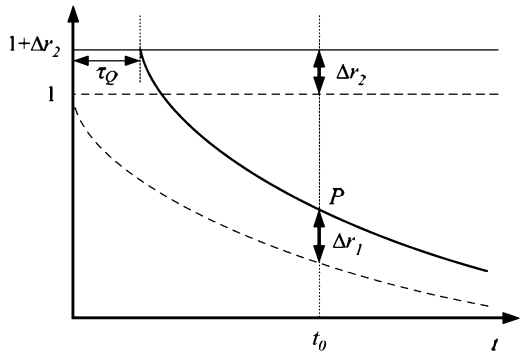


Fig. 3. Quantization error introduced by the proposed solution.

$\tilde{r}_{E,2}(t)$ since the input of the peak detectors is now connected to ground. Thus, $\tilde{r}_{E,1}(t)$ and $\tilde{r}_{E,2}(t)$ decrease from the first-peak value with time constants $\tau_{E,1}$ and $\tau_{E,2}$, respectively, and are sampled with sampling time $T_s$. If $\tau_{E,2} \gg \tau_{E,1}$ (this can be simply obtained by replacing $R_{E,2}$ with an open circuit, which implies $\tau_{E,2} \to \infty$), the TOA can be reconstructed from the first pair of samples after the trigger, as shown in Fig. 2. In this case, calling $r_1[1]$ and $r_2[1]$ the first samples taken at sampling instant $t_s$ at the output of the samplers of $B1$ and $B2$, respectively, the random delay $t_0$ (uniformly distributed in $[0, T_s]$) with respect to the (unknown) TOA of the first peak can be determined by solving the following:

$$r_2[1]\exp(-t_0/\tau_{E,1}) = r_1[1]. \tag{5}$$

The TOA of the first peak is then simply given as $\tau = t_s - t_0$.

At time $T_{B_{01}}$, a reset pulse from the timer sets the switches $S_{B,1}$ and $S_{B,2}$ to their short-circuit position, which causes a discharge of $C_{E,1}$ and $C_{E,2}$. At time $T_{B_{10}}$, $S_{B,1}$ and $S_{B,2}$ are switched back to the original open-circuit position. Finally, at $T_{A_{10}}$, $S_A$ is also reset by the timer to its original open-circuit position, and the circuit can repeat the described procedure. For proper operation, $T_{B_{01}} \geq T_s$, to allow to collect at least one sample needed to estimate $t_0$, and $T_{A_{10}} \geq \tau_{\mathrm{cds}}$, to avoid detection of late multipath components corresponding to a previous transmission; this way, repetitive transmission of pulses separated by at least $T_{A_{10}}$ is possible.

There are two sources of inaccuracy that make TOA estimation with this scheme different from that of a classical first-peak detector based on Nyquist sampling and perfect reconstruction of the received signal envelope. The first is the quantization error introduced by the two samplers, and the second is due to possible fluctuations in the actual decay constant $\tau_{E,1}$ from its nominal value (typically caused by temperature variations). In the following, these error sources are evaluated.

By solving the following:

$$\exp(-t_0/\tau_{E,1}) + \Delta r_1 = (1+\Delta r_2)\exp\left(\frac{-(t_0-\tau_Q)}{\tau_{E,1}(1+\Delta\tau_{E,1})}\right) \tag{6}$$

in point $P$, as shown in Fig. 3, the error $\tau_Q$ in the TOA estimation can be determined. Here, $\Delta r_1$ and $\Delta r_2$ are the quantization errors of the samplers of $B1$ and $B2$, respectively, and $\Delta\tau_{E,1}$ is the relative error in the decay constant $\tau_{E,1}$. Under the hypothesis that the error $\tau_Q \ll \tau_{E,1}$ (which is true, according to the values given in the following) and considering only first-order errors, $\tau_Q$ can be approximated as

$$\begin{aligned}\tau_Q \approx& \tau_{E,1}\left(-\Delta r_2 + \Delta r_1 \exp(t_0/\tau_{E,1}) - \Delta\tau_{E,1} t_0/\tau_{E,1}\right)\\ \approx& \tau_{E,1}\left(-\Delta r_2 + \Delta r_1 \exp(t_0/\tau_{E,1})\right)\end{aligned} \tag{7}$$

since $\Delta\tau_{E,1}$ can be easily made negligible [if $\Delta\tau_{E,1} \leq 10^{-4}$, from (7)] with an inexpensive calibration step by piloting the input with a known voltage. For evaluating $\tau_Q$, we assume that the first-peak level is approximately equal to the maximum ADC input level. In this case, fixing the interval of variation of the ADC input between 0 and the estimated first-peak level, the quantization errors $\Delta r_1$ and $\Delta r_2$ normalized to the first-peak level are uniformly distributed random variables (RVs) in $[-1/2^{N_s+1}, 1/2^{N_s+1}]$, where $N_s$ is the number of bits of the ADC. $\tau_Q$ is then a zero-mean RV. By applying the variance propagation law to the equation for $\tau_Q$, approximated to the second order and linearized around the mean of $\Delta r_1$, $\Delta r_2$, and $t_0$, its variance is

$$\sigma^2_{\tau_Q} \approx \frac{\tau^2_{E,1}}{12 \cdot 2^{2N_s}}\left(1 + \exp(T_s/\tau_{E,1})\right). \tag{8}$$

The minimum of (8) with respect to $\tau_{E,1}$ is found by putting its derivative equal to zero and solving the resulting equation with respect to $T_s/\tau_{E,1}$. Using the obtained value $T_s/\tau_{E,1} \approx 2.217$ in (8) results in $\sigma_{\tau_Q} \approx 0.42 \cdot T_s/2^{N_s}$, which depends on the performance of the sampler. For example, with $T_s = 20$ ns (a sample rate of 50 MHz) and $N_s = 8$, $\sigma_{\tau_Q}$ causes a range error of about 1 cm. Thus, the proposed receiver allows to significantly relax the hardware requirements compared with Nyquist-based approaches due to the limited amount of signal processing and the low sampling rate of a few tens of megahertz, which can be easily realized with inexpensive ADCs currently available. In this way, the main implementation challenges for UWB TOA-based ranging are solved. At the same time, the error specifically introduced by the proposed receiver is on the order of 1 cm, which is often negligible for practical applications and comparable with that of an ideal first-peak detector with perfect knowledge of the received signal envelope. In addition, this is a large improvement when compared with, e.g., traditional bin-energy-based TOA estimation approaches [11], which achieve lower complexity by sacrificing part of the potential accuracy available.

### B. TOA Estimation Strategy

The receiver proposed in Section III-A directly estimates the TOA from the received signal without further processing. Therefore, it is not possible to increase the effective SNR by performing an average *before* TOA estimation to allow for performance and reliability flexibility. To address this issue, a statistical TOA estimation strategy, in which the TOA measurements of multiple transmitted pulse signals are combined, is proposed and analyzed in the following.

A set of $N$ estimated TOAs, obtained from $N$ repetitively transmitted pulses, are temporally sorted. The strategy now is to find the first time window of duration $T_W$ and arbitrary starting time, which contains at least $N_{\mathrm{TH}}$ of these TOAs, as shown in

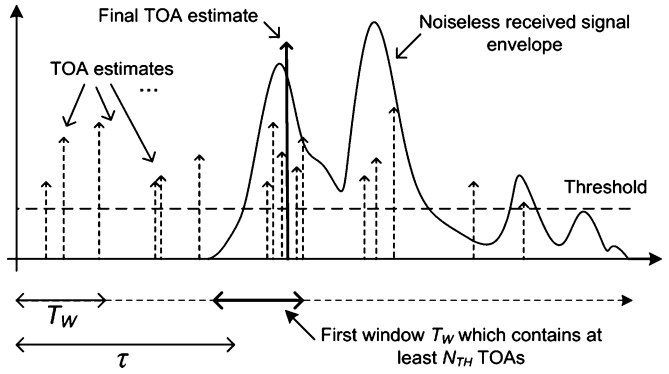


Fig. 4. TOA estimation strategy.

Fig. 4. The average of the TOAs in this window is chosen as the final TOA estimate.

The performance of this approach is analyzed by evaluating the probability of *early false alarm* (EFA) $P_{\mathrm{EFA}} \triangleq \Pr$ {in the initial noise-only part of $N$ received signals of duration $\tau$, there exists at least one time window of duration $T_W$, which contains at least $N_{\mathrm{TH}}$ TOAs} and the probability of *missed detection* (MD) $P_{\mathrm{MD}} \triangleq (1 - P_{\mathrm{EFA}}) \cdot \Pr$ {in the $N$ TOA estimates, there are less than $N_{\mathrm{TH}}$ TOAs in *any* time window of duration $T_W$, which contains the *true* TOA of the direct path[1]}. If $P_{\mathrm{EFA}} \ll 1$, then $P_{\mathrm{MD}} \approx \Pr$ {In $N$ transmissions, there are less than $N_{\mathrm{TH}}$ TOAs in any time window of duration $T_W$, which contains the true TOA of the direct path}. In this way, the reliability of the TOA estimation can be evaluated. We will show that if the direct path is correctly detected, the range error is at centimeter level, corresponding to the very large bandwidths used.

To simplify the analysis of the theoretical evaluation of $P_{\mathrm{EFA}}$ and $P_{\mathrm{MD}}$, we assume that the receiver implements a first crossing detection over a threshold $r_{\mathrm{TH}}$ instead of a first-peak detection. Due to the short duration of the used pulse, the difference between the two cases is negligible. The threshold $r_{\mathrm{TH}}$ is related to the noise power of the received signal at the matched filter output and is expressed as $r_{\mathrm{TH}} = k_{\mathrm{TH}}\sigma_{n_{\mathrm{MF}}}$, where $k_{\mathrm{TH}}$ is a real positive number and $\sigma^2_{n_{\mathrm{MF}}} = \int_{-\infty}^{\infty} N_0|W(f)|^2/E_w df = N_0$ is the variance of the noise $n_{\mathrm{MF}}(t)$ at the unity-gain matched filter output, with $W(f)$ being the Fourier transform of the pulse $w(t)$ given in (3).

### C. Performance Evaluation: Early False Alarm

Since the calculation of the exact expression for $P_{\mathrm{EFA}}$ is difficult, an upper bound is determined. The first problem is that the duration $\tau$ of the noise-only part of the received signal is an unknown RV. Since $P_{\mathrm{EFA}}$ monotonically increases with $\tau$, a noise time window $\tau_{\mathrm{MAX}} = \max\{\tau\}$ is considered. The actual value of this $\tau_{\mathrm{MAX}}$ depends on the particular choice of the parameters in the coarse acquisition step. For the simulation results presented here, a choice of $\tau_{\mathrm{MAX}} = 160$ ns is used, corresponding to the parameters selected for the coarse acquisition step, as discussed in Section V. The second problem is related to the distribution of the estimated TOA within $\tau$. Reference [24] provides a framework to evaluate the probability $p_N(T_n)$ of the first-level crossing in a time window $T_n$ when only Gaussian noise is present and using a double-sided threshold (symmetric about zero), whereas reference [25] applies these results to UWB ranging. These results can be used in our analysis, observing that $p_N(T_n)$ also represents the probability of a single-sided (above zero) first threshold crossing for the noise *envelope* at the matched filter output.[2]

From [24], the single-sided threshold first crossing probability in $T_n$ for a Gaussian process is $G(T_n) = 1 - \exp(-T_n/\rho)$, with $\rho = 2\Phi(k_{\mathrm{TH}})/\lambda \exp(k^2_{\mathrm{TH}}/2)$ and $\lambda = 2\sqrt{\int_{-\infty}^{\infty} f^2 S_{nw}(f)df / \int_{-\infty}^{\infty} S_{nw}(f)df}$, where $\Phi(x) = \int_{-\infty}^{x} 1/\sqrt{2\pi}\exp(-\xi^2/2)d\xi$ and $S_{nw} = N_0 W^2(f)$ is the noise power spectral density at the matched filter output. From $G(T_n)$, an upper bound $\bar{p}_N(T_n)$ for the required probability can be calculated as [24] $p_N(T_n) \le \bar{p}_N(T_n) = 1 - (1 - G(T_n))^2$.

Observing that the Fourier transform of the considered pulse $w(t)$ in (3) is

$$W(f) = A_0 T_g \sqrt{\pi/2}\left(\exp\left(-2T_g^2\pi^2(f - f_0)^2\right) + \exp\left(-2T_g^2\pi^2(f + f_0)^2\right)\right) \quad (9)$$

gives $\lambda = 2\sqrt{f_0^2 + 1/(8T_g^2\pi^2)}$. By plotting the cumulative distribution function of $p_N(T_n)$, for the considered values of $T_n$, $p_N(T_n)$ approximately linearly increases with $T_n$ when choosing $k_{\mathrm{TH}} \approx 4$ or larger, showing that, in case a TOA estimation occurs in the time window $T_n$, it can be assumed uniformly distributed in $[0, T_n]$. This means that, for $k_{\mathrm{TH}} \ge 4$ and putting $T_n = \tau_{\mathrm{MAX}}$

$$P_{\mathrm{EFA}} \le \sum_{n=N_{\mathrm{TH}}}^{N} P_0(n)\binom{N}{n}\bar{p}_N^n(\tau_{\mathrm{MAX}})\left(1 - \bar{p}_N(\tau_{\mathrm{MAX}})\right)^{N-n} \quad (10)$$

where $P_0(n) = \Pr$ {Given $n$ uniformly distributed RVs in $[0, \tau_{\mathrm{MAX}}]$, there exists at least one time window $T_W$, which contains at least $N_{\mathrm{TH}}$ threshold crossings}. A closed-form expression for $P_0(n)$ is difficult to derive. For this reason, its value has been determined by simulation.

There are four parameters in (10) that determine $P_{\mathrm{EFA}}$. $T_W$ should be chosen as small as possible since $P_{\mathrm{EFA}}$ increases with $T_W$. Its value has been chosen equal to 1.5 ns, according to the motivations provided in Section III-D. The threshold $k_{\mathrm{TH}}$ is a parameter that affects both $P_{\mathrm{EFA}}$ and $P_{\mathrm{MD}}$. Since only bounds for $P_{\mathrm{EFA}}$ and $P_{\mathrm{MD}}$ are given, it is not possible to find the $k_{\mathrm{TH}}$ that minimizes the overall probability of EFA and MD. However, in a relatively wide range of $k_{\mathrm{TH}}$ (between about 3.5 and 5.5), the overall probability does not significantly change (using

[1]Due to multipath and propagation through dielectric materials, the (unknown) true TOA of the direct path does not necessarily coincide with the TOA of the first peak of the received signal, even in noiseless conditions [5].

[2]In fact, it can be noted that the signal envelope is always larger than or equal to the absolute value of the signal itself, and if the envelope crosses a single-sided threshold in one point, it also crosses a double-sided threshold within a time interval equal to the inverse of the carrier frequency $f_0$, around that point. According to these points and observing that the values $T_n$ of interest are $T_n \gg 1/f_0$, in a window $T_n$, the double-sided first threshold crossing probability for the noise at the matched filter output is equal to the single-sided first threshold crossing probability of the noise envelope at the matched filter output. This justifies the use of the results in [24] for the considered problem.

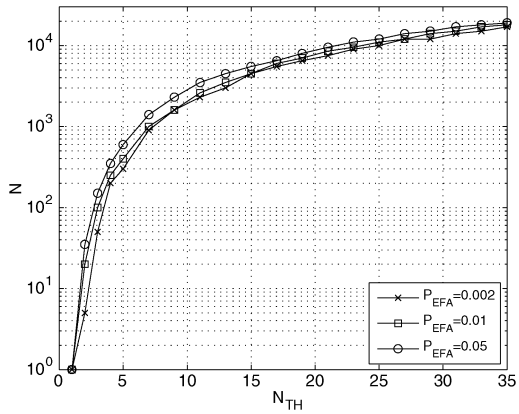


Fig. 5. Region of the plane $(N, N_{\rm TH})$ that satisfies the required $P_{\rm EFA} \leq P_{\rm EFA}^{\rm req}$ (below the curves), for $P_{\rm EFA}^{\rm req} = 0.002, 0.01, 0.05$.

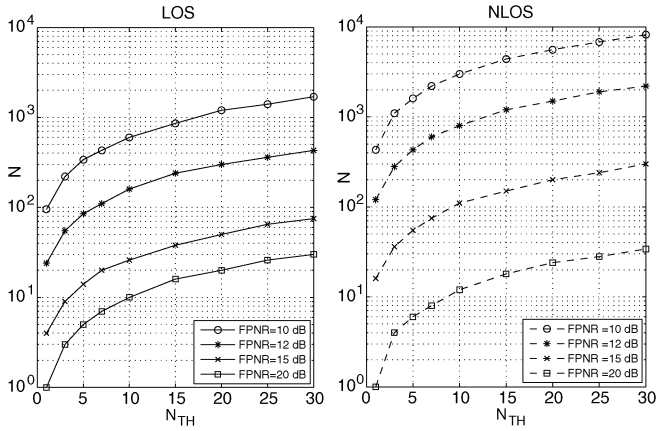


Fig. 6. Regions of the plane $(N, N_{\rm TH})$ that satisfy the required $P_{\rm MD} \leq 0.01$ for different FPNR (above the curves), on the left for $\sigma_{S_{\rm FP}} = 1$ dB (LOS) and on the right for $\sigma_{S_{\rm FP}} = 4.5$ dB (NLOS).

the corresponding set of system parameters); for this reason, $k_{\rm TH} = 4.5$ is chosen. The other parameters to select in (10) are $N$ and $N_{\rm TH}$. Varying both of them and calculating $P_{\rm EFA}$ for each pair $(N, N_{\rm TH})$, it is possible to determine a region in the $(N, N_{\rm TH})$ plane, which satisfies a target $P_{\rm EFA}^{\rm req}$. Fig. 5 shows the region of the $(N, N_{\rm TH})$ plane, which satisfies the requirement $P_{\rm EFA} \leq P_{\rm EFA}^{\rm req}$ for $P_{\rm EFA}^{\rm req} = 0.002$, 0.01, and 0.05, as examples. The area $(N, N_{\rm TH})$ below the respective curve allows $P_{\rm EFA}$ to be smaller than the target $P_{\rm EFA}^{\rm req}$. As expected, this area becomes smaller for decreasing $P_{\rm EFA}$; however, significant variations in the target $P_{\rm EFA}^{\rm req}$ can be obtained with limited variation in the parameters $(N, N_{\rm TH})$ since the plotted curves are very close to each other. In this way, significant flexibility in the system performance can be achieved.

### *D. Performance Evaluation: Missed Detection*

From the definition of $P_{\rm MD}$, the following upper bound is straightforward: $P_{\rm MD} \leq \Pr$ {in $N$ TOA estimates, there are less than $N_{\rm TH}$ estimates in *a particular* time window $W_0$ of duration $T_W$ which contains the true TOA} since this last event is included in that which specifies $P_{\rm MD}$. For space reasons, we omit here the justifications for the choice of $W_0$, which allows easy calculation of the bound, and we refer to [26] for more details. In [26], we show that choosing $T_W \approx 1.5$ ns results in $P_{\rm MD} \leq \sum_{n=0}^{N_{\rm TH}-1} \binom{N}{n} p_D^n (1-p_D)^{N-n}$, where $p_D \triangleq \Pr$ {the first-peak received signal plus the noise that crosses the threshold}. Now, $p_D = \Pr\{|a_{\rm pk} + n_{\rm MF}(t_{\rm pk})| \geq k_{\rm TH}\sigma_{n_{\rm MF}}\} = \Pr\{|a_{\rm pk}/\sigma_{n_{\rm MF}} + R_0| \geq k_{\rm TH}\} = \Pr\{|\sqrt{\rm FPNR \cdot S_{FP}} + R_0| \geq k_{\rm TH}\} \geq \Pr\{\sqrt{\rm FPNR \cdot S_{FP}} + R_0 \geq k_{\rm TH}\} = 1 - \Phi(k_{\rm TH} - \sqrt{S_{\rm FP} \cdot \rm FPNR})$, with $a_{\rm pk}$ and $t_{\rm pk}$ being the first-peak amplitude and its TOA, respectively, at the matched filter output in noiseless conditions; $R_0 = n_{\rm MF}/\sigma_{n_{\rm MF}}$ being the standard Gaussian distributed RV; $\rm FPNR = E_w/(N_0 L_{FP})$ being the first-peak power-to-noise ratio, as expected from the link budget; and $L_{\rm FP}$ is the first-peak power path loss.[3] $S_{\rm FP}$ is the first-peak power fading. These variations are due to the partial overlap of the direct path with later multipath components and distortions undergone by the direct path itself, which typically happen in NLOS propagation. The upper bound for $P_{\rm MD}$ results in

$$P_{\rm MD} \leq \sum_{n=0}^{N_{\rm TH}-1} \binom{N}{n} \int_{s=-\infty}^{\infty} f_{S_{\rm FP}}(s)\,(1-z(s))^n\, z^{N-n}(s) ds \quad (11)$$

where $f_{S_{\rm FP}}(s)$ is the probability density function (pdf) of the first-path power fading, and $z(s) = \Phi(k_{\rm TH} - \sqrt{s \cdot \rm FPNR})$. Unfortunately, the IEEE models [28] do not provide an accurate statistical characterization for $S_{\rm FP}$. For this reason, results in [27] are used to evaluate (11), where a characterization of $S_{\rm FP}$ for typical indoor office environments is provided. It is shown that it can be modeled as a zero-mean log-normal RV with standard deviation $\sigma_{S_{\rm FP}}$, which depends on the bandwidth. For example, for $B = 3$ GHz, $\sigma_{S_{\rm FP}} \approx 1$ dB in LOS, and $\sigma_{S_{\rm FP}} \approx 4.5$ dB in NLOS.

Fig. 6 shows an example of the regions (above the curves) of the $(N, N_{\rm TH})$ plane, which satisfy $P_{\rm MD} \leq 0.01$ obtained by evaluating (11) both for $\sigma_{S_{\rm FP}} = 1$ dB (LOS) in the left-hand figure, and for $\sigma_{S_{\rm FP}} = 4.5$ dB (NLOS) in the right-hand figure, and for different values of FPNR. It can be seen that, for the same FPNR and $N_{\rm TH}$, NLOS propagation requires a larger $N$, i.e., the number of estimated TOAs, for meeting a required $P_{\rm MD}$ due to the larger first-path power fading. This effect is particularly evident for small values of FPNR and becomes negligible for larger ones.

From the results on the EFA and MD analysis, it is now possible to determine the region $(N, N_{\rm TH})$ that satisfies the combined requirements on $P_{\rm EFA}$ and $P_{\rm MD}$. For example, in Figs. 5 and 6, it can be seen that for having $P_{\rm EFA} \leq 0.01$ and $P_{\rm MD} \leq 0.01$, by choosing $N = 3$ and $N_{\rm TH} = 2$, the minimum required FPNR is 20 dB, both for LOS and for NLOS. Having $\rm FNPR = 10$ dB requires at least $N = 500$ and $N_{\rm TH} = 7$ for LOS, whereas $N = 5000$ and $N_{\rm TH} = 17$ for NLOS. A smaller FPNR is possible; however, this needs a substantial increase in $N$. The required FPNR allows calculation of the coverage of the proposed solution, as discussed in Section VI.

To evaluate the achieved accuracy, the mean absolute range error obtained with the proposed receiver has been investigated

[3]Note that $L_{\rm FP}$ usually differs from the total signal power path loss, as discussed in more detail in Section VI; this difference is neglected in the IEEE UWB channel models [28].

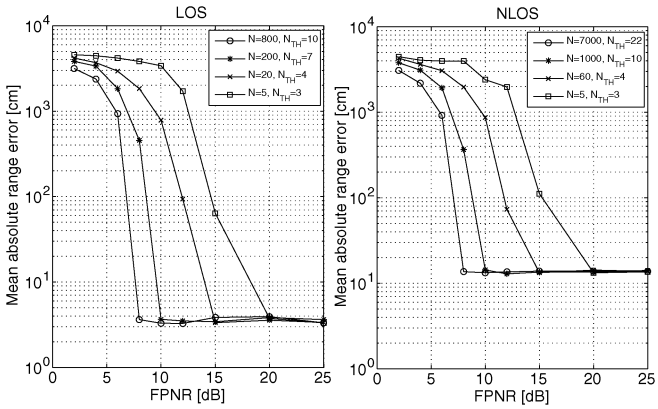


Fig. 7. Mean absolute range error in centimeters versus FPNR, both for (left) LOS and for (right) NLOS for different pairs of $(N, N_{\mathrm{TH}})$.

using measured UWB channel responses collected during a measurement campaign in which a large set of channel responses were measured in the time domain using UWB pulse signals. Details on the measurement setup and environment can be found in [5]. For the simulation, a measured channel response is randomly chosen from the total available set of measurements. The selected signal, which can be considered noise free, is filtered in the proper 3-GHz bandwidth. The total frame duration is chosen as $T_f = 800$ ns, and the noise-only part $\tau = \tau_{\mathrm{MAX}} = 160$ ns, in line with the values given in Section V on coarse acquisition. A signal format such as in (1) is built, and noise is artificially added to obtain the proper value of FPNR. The distance estimated with the proposed receiver is compared with the measured distance between transmitter and receiver. The results are averaged over 100 different measurements randomly chosen from the total set. By choosing a proper pair $(N, N_{\mathrm{TH}})$ that allows neglect of $P_{\mathrm{EFA}}$ and $P_{\mathrm{MD}}$ for FPNR = 10, 12, 15, and 20 dB, respectively, it is possible to investigate the achievable range accuracy. Results in Fig. 7 show that centimeter-level accuracy can be obtained when the FPNR satisfies the requirements in Figs. 5 and 6. Similar accuracies were found from simulations using the IEEE models (4 cm for CM3 and 7 cm for CM4), where the range error was defined as the difference between the TOA of the first path of the (infinite bandwidth) CIR and the TOA estimated from the received signal with the proposed solution.

## IV. Narrowband Interference Analysis

Since UWB is used unlicensed in already occupied frequency spectrum, the effect of interference from narrowband signals is an important issue. Here, the effect of NBI on the proposed peak-detector-based TOA estimation technique is evaluated. The NBI is modeled as a single-tone continuous-wave signal as follows:

$$i(t) = \alpha_I A_I \cos(2\pi f_I t + \theta_I) \tag{12}$$

where $A_I^2/2$ is the average NBI power, $\alpha_I$ is a Rayleigh distributed RV, which accounts for the slowly varying narrowband fading, with $E[\alpha_I^2] = 1$, and $\theta_I$ is a random phase uniformly distributed in $[0, 2\pi]$. This model has been widely adopted in literature [12]–[16] since a narrowband interfering signal can be realistically considered constant for several UWB frames and can be used as a benchmark to compare NBI impairments on different techniques. To keep the analytical approach to the problem feasible, the NBI signal phase $\theta_I$ is assumed independent from frame-to-frame, which is reasonable since $2\pi f_I T_f \approx 10^4$. On the contrary, a particular realization of $\alpha_I$ can be considered constant in all the frames belonging to one complete set of $N$ transmissions since the channel coherence time is usually significantly longer.

### A. Performance Evaluation: Early False Alarm

The evaluation of the probability of *EFA* under NBI can be reconducted to the calculation of the probability of the first crossing of a time-varying threshold for stationary Gaussian processes. In [17], a theoretical framework is presented, which provides an approximate solution for the first crossing detection probability for Gaussian noise and general time-varying thresholds and a closed-form solution for periodic thresholds. The results of this approximation are very accurate for first crossing probabilities less than 0.1 in the considered noise-only time window $T_n$, which is the situation of interest here. Specific results for an asymptotically periodic threshold are reported in [18]. This is an interesting case for the problem considered here since a sinusoidal signal is a particular case of an asymptotically periodic threshold. The problem can be solved with an approach similar to that presented in Section III-C, considering a periodic threshold $b(t) = i_{\mathrm{MF}}(t) + r_{\mathrm{TH}}$,[4] where $i_{\mathrm{MF}}(t) = i(t) \otimes w(-t)/\sqrt{E_w} = K_W(f_I)/\sqrt{B}\alpha_I A_I \cos(2\pi f_I t + \arg\{W(f_I)\})$ is the interference at the matched filter output. Here, $\otimes$ is the convolution operator, $K_W(f_I)$ is defined as $K_W(f_I) \triangleq |W(f_I)|/|W_{\mathrm{sinc}}(f_I)|$, and $W_{\mathrm{sinc}}(f)$ is the Fourier transform of a sinc function with a bandwidth $B$ centered around $f_0$ and energy $E_w$. Conditioned to a given value $n_{\mathrm{MF}}(0) \le b(0)$ of the noise at $t = 0$ at the matched filter output, from [18], we find that the single-sided first crossing pdf for $b(t)$ is

$$g\left(t|n_{\mathrm{MF}}(0)\right) = R\left[b(t)\right] \exp\left(-\int_0^t R\left[b(t')\right] dt'\right) \tag{13}$$

where $R[b(t)]$ is a periodic function given by

$$R\left[b(t)\right] = \frac{\sqrt{-\ddot{\gamma}(0)}}{2\pi} \exp\left(\frac{-\left(r_{\mathrm{TH}} + i_{\mathrm{MF}}(t)\right)^2}{2\sigma^2_{n_{\mathrm{MF}}}}\right) \cdot \left(\exp\left(\frac{\dot{i}^2_{\mathrm{MF}}(t)}{2\ddot{\gamma}(0)}\right) - \dot{i}_{\mathrm{MF}}(t)\sqrt{\frac{2\pi}{-\ddot{\gamma}(0)}} \times \left(1 - \Phi\left(\frac{\dot{i}_{\mathrm{MF}}(t)}{\sqrt{-\ddot{\gamma}(0)}}\right)\right)\right) \tag{14}$$

[4]Note that the original problem requires calculating the first time in $[0, \tau]$ in which $n_{\mathrm{MF}}(t) + i_{\mathrm{MF}}(t) = r_{\mathrm{TH}}$; however, since the process is stationary and results in $i_{\mathrm{MF}}(t) = -i_{\mathrm{MF}}(t + \pi/(2\pi f_I))$, this is statistically equivalent to calculating the first time in $[0, \tau]$ in which $n_{\mathrm{MF}}(t) = r_{\mathrm{TH}} + i_{\mathrm{MF}}(t)$.

where $\gamma(t)$ is the normalized autocorrelation function of $n_{\mathrm{MF}}(t)$, and $\{\dot{\cdot}\}$ and $\{\ddot{\cdot}\}$ represent the first- and second-time derivatives of $\{\cdot\}$, respectively. The conditioned single-sided first crossing probability in $T_n$ can now be calculated as $G(T_n|n_{\mathrm{MF}}(0)) = \int_0^{T_n} g(t|n_{\mathrm{MF}}(0))dt$ and the probability of single-sided first threshold crossing as

$$\begin{aligned} G(T_n) &= \Pr\{n_{\mathrm{MF}}(0) \geq b(0)\} + G\left(T_n|n_{\mathrm{MF}}(0) \leq b(0)\right) \\ &\approx G\left(T_n|n_{\mathrm{MF}}(0) \leq b(0)\right) \\ &= \int_{\theta=0}^{2\pi} \int_{n_{\mathrm{MF}}(0)=-\infty}^{b(0)} G\left(T_n|n_{\mathrm{MF}}(0)\right) f_{\theta_I}(\theta) f_{n_{\mathrm{MF}}}(n) dn d\theta \\ &= \frac{1}{2\pi} \int_0^{2\pi} G\left(T_n|n_{\mathrm{MF}}(0)\right) \\ &\quad \cdot \Phi\left(\frac{r_{\mathrm{TH}} + \alpha_I A_I K_W(f_I)\cos\theta/\sqrt{B}}{\sigma_{n_{\mathrm{MF}}}}\right) d\theta \end{aligned} \tag{15}$$

where it has been used that $G(T_n|n_{\mathrm{MF}}(0))$ does not depend on the particular $n_{\mathrm{MF}}(0)$ given $n_{\mathrm{MF}}(0) \leq b(0)$; therefore, it can be taken out of the internal integral in the second line of (15). To calculate (15), $\Pr\{n_{\mathrm{MF}}(0) \geq b(0)\}$ has been neglected; this is licit since it is significantly smaller than $G(T_n|n_{\mathrm{MF}}(0) \leq b(0))$. Since we are interested in $T_n$ and $r_{\mathrm{TH}}$ such that $T_n B \gg 1$ and $G(T_n) \ll 1$, which makes crossing inside a window $T_n$ much more likely than in $t = 0$. As for the case without NBI, an upper bound for the required double-sided first crossing probability is $p_N(T_n) \leq \bar{p}_N(T_n) = 1 - (1 - G(T_n))^2$. Now, the upper bound for $P_{\mathrm{EFA}}$ under NBI is given by

$$\begin{aligned} P_{\mathrm{EFA}} \leq \sum_{n=N_{\mathrm{TH}}}^{N} P_0(n) \binom{N}{n} \int_0^{\infty} f_{\alpha_I}(\alpha) \bar{p}_N^n(\tau_{\mathrm{MAX}}) \\ \cdot \left(1 - \bar{p}_N(\tau_{\mathrm{MAX}})\right)^{N-n} d\alpha \end{aligned} \tag{16}$$

It is interesting to compare the results that can be obtained from (13)–(15) for the particular case of $i(t) = 0$ with those without NBI of Section III-C. By using the differentiation theorem $\ddot{\gamma}(0) = -\int_{-\infty}^{\infty}(2\pi f)^2 S_{nw}(f)df / \int_{-\infty}^{\infty} S_{nw}(f)df = -2\pi^2\lambda^2$, $R[b(t)] = \lambda/\sqrt{2}\exp(-r_{\mathrm{TH}}^2/2\sigma_{n_{\mathrm{MF}}}^2)$ becomes a constant, and we find $G(T_n) = (1 - \exp(-T_n/\rho))\Phi(k_{\mathrm{TH}})$. Observing that for the $k_{\mathrm{TH}}$ of interest $\Phi(k_{\mathrm{TH}}) \approx 1$, this expression for $G(T_n)$ equals that provided in Section III-C.

### B. Performance Evaluation: Missed Detection

With arguments similar to those discussed in Section III-C, a lower bound for $p_D$ conditioned to a particular realization of $i(t)$ is $p_D \geq \Pr\{\sqrt{\mathrm{FPNR}\cdot S_{\mathrm{FP}}} + R_0 \geq k_{\mathrm{TH}} + i_{\mathrm{MF}}(t_{\mathrm{pk}})/\sigma_{n_{\mathrm{MF}}}\} = 1 - \Phi(k_{\mathrm{TH}} + i_{\mathrm{MF}}(t_{\mathrm{pk}})/\sigma_{n_{\mathrm{MF}}} - \sqrt{S_{\mathrm{FP}}\cdot\mathrm{FPNR}})$. Averaging over $\theta_I$ results in

$$\begin{aligned} p_D \geq \bar{p}_D = 1 - \frac{1}{2\pi}\int_0^{2\pi} \Phi\left(k_{\mathrm{TH}} + \frac{\alpha_I A_I K(f_I)\cos\theta}{\sigma_{n_{\mathrm{MF}}}\sqrt{B}} \right. \\ \left. - \sqrt{S_{\mathrm{FP}}\cdot\mathrm{FPNR}}\right) d\theta \end{aligned} \tag{17}$$

where $\bar{p}_D$ is the lower bound of $p_D$. The upper bound for the probability of MD can be written as

$$\begin{aligned} P_{\mathrm{MD}} \leq \sum_{n=0}^{N_{\mathrm{TH}}-1} \binom{N}{n} \int_0^{\infty}\int_0^{\infty} \bar{p}_D^n (1-\bar{p}_D)^{N-n} \\ \cdot f_{S_{\mathrm{FP}}}(s) f_{\alpha_I}(\alpha) d\alpha ds \end{aligned} \tag{18}$$

### C. TOA Performance Evaluation Under NBI

With NBI being present, the impairments in $P_{\mathrm{EFA}}$ and $P_{\mathrm{MD}}$ can now be evaluated using (17) and (18) for a given set of $(N, N_{\mathrm{TH}})$ and $k_{\mathrm{TH}}$. To compare the performance for the cases with and without NBI, the parameters of interest have to be chosen in a meaningful way. In the following, matching of the threshold $k_{\mathrm{TH}}$ is used to obtain the same $P_{\mathrm{EFA}}$ for the noise-plus-interference window as for the case without NBI, i.e., the value of $k_{\mathrm{TH}}$ for the required EFA probability is determined while keeping the other system parameters constant. The corresponding values of $(N, N_{\mathrm{TH}})$, which satisfy the requested $P_{\mathrm{MD}}$, are accordingly calculated. Fig. 8 shows the regions of the $(N, N_{\mathrm{TH}})$ plane, which satisfy $P_{\mathrm{EFA}} \leq 0.01$ and $P_{\mathrm{MD}} \leq 0.01$, for $\sigma_{S_{\mathrm{FP}}} = 1$ dB (corresponding to LOS), for different values of the interference-to-noise ratio ($\mathrm{INR} \triangleq A_I^2/(2N_0B)$), and for FPNR = 12, 15, and 20 dB, for comparison. In a similar way, results for the NLOS case can be determined. The curve corresponding to the constraint for the $P_{\mathrm{EFA}}$ is the same as for the case without NBI, due to the EFA probability matching criterion used. By evaluating the variations in the curve for $P_{\mathrm{MD}}$ for a given value of INR and FPNR, it is possible to obtain the corresponding impairment in terms of the minimum

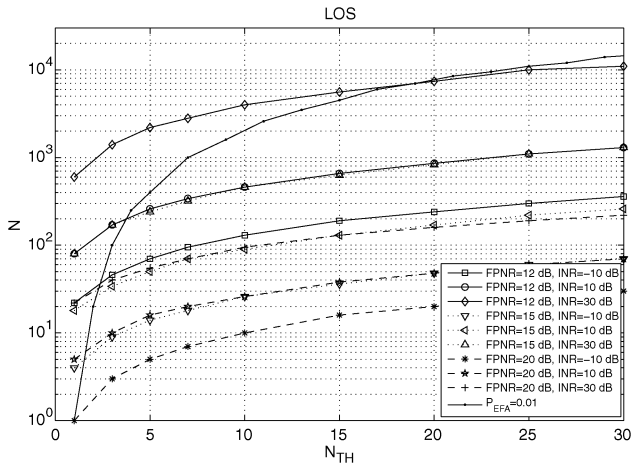


Fig. 8. Regions of the plane $(N, N_{\mathrm{TH}})$ that satisfy the required $P_{\mathrm{EFA}} \leq 0.01$ and $P_{\mathrm{MD}} \leq 0.01$, for different values of FPNR and INR, and for $\sigma_{S_{\mathrm{FP}}} = 1$ dB (LOS). Suitable values of $N$ are below the $P_{\mathrm{EFA}}$ curve and above the $P_{\mathrm{MD}}$ curves.

required $N$ (and $N_{\mathrm{TH}}$) or FPNR. From the figure, an increase in INR requires an increase in the minimum required $N$ for the same FPNR, e.g., for FPNR = 12 dB, the minimum $N$ increases from about 60, without interference, to about 7000 for INR = 30 dB. These values can be found by looking for the point $(N, N_{\mathrm{TH}})$ with the minimum $N$ which is both below the curve for $P_{\mathrm{EFA}}$ and above the curve for $P_{\mathrm{MD}}$ in the two cases, for the same FPNR. In a similar way, the impairments can also be evaluated in terms of the minimum required FPNR, for the same $(N, N_{\mathrm{TH}})$. For example, for $(N = 60, N_{\mathrm{TH}} = 3)$, the minimum required FPNR in the absence of NBI is about 12 dB (see Figs. 5 and 6). An interference source with INR = 30 dB requires an increase in the FPNR to about 20 dB, to meet the same performance requirements (see Fig. 8).

## V. Coarse Acquisition

Next, a coarse acquisition strategy, required for proper operation of the receiver presented in Section III-A, is described. The purpose of this step is to provide an estimate $T_0$ of the frame starting time, such that the first-peak crosses the threshold at $\tau_0 = T_0 + \tau$ (which was accurately estimated in Section III with respect to $T_0$) with $0 \le \tau \le T_f - \tau_{\mathrm{cds}}$. To keep the system complexity low, this coarse acquisition is based on energy detection, which is a well-known technique. However, different from the considered schemes as presented in, e.g., [19]–[21], a novel theoretical framework is presented here to calculate the statistics of the maximum energy bin in closed form, which allows evaluation of the performance of the scheme in terms of probability of acquisition and to simply relate it to the relevant system and channel parameters.

Fixing an arbitrary observation start time and choosing the number $K$ of time bins per frame with duration $T = T_f/K$, the following energy statistics for each $k$th bin are calculated:

$$E_k = \sum_{j=0}^{N_{\mathrm{CA}}-1} \int_{kT+jT_f}^{(k+1)T+jT_f} r(t)^2 dt \tag{19}$$

for $k = 0 \ldots K-1$. $N_{\mathrm{CA}}$ is the number of frames used in this step. The coarse estimation of the frame starting time is calculated as

$$T_0 = T\left(\arg\max_k\{E_k\} - 1\right). \tag{20}$$

The rationale behind this strategy is the following. Assuming a bin duration $T \approx \tau_{\mathrm{cds}}$ (the appropriateness of this choice will be discussed), in the most general situation, there are two bins in a frame $T_f$, which are called $s_1$ and $s_2$, and which contain the first and the last part of the useful signal, respectively, and $K-2$ bins, i.e., $n_1 \ldots n_{K-2}$, containing only noise (see also Fig. 9). Since the strategy outlined in (19) and (20) performs a maximum energy detection (summed over $N_{\mathrm{CA}}$ frames), it is likely that the maximum energy bin is the one corresponding to $s_1$ or $s_2$. The start time of the signal with respect to $T_0$ (assumed for notational convenience equal to zero) is then $\tau = T + T_R$ or $\tau = T_R$ if the maximum energy bin is $s_1$ or $s_2$, respectively, where $T_R$ is the delay of the first path from $T_0$ modulo $T$,

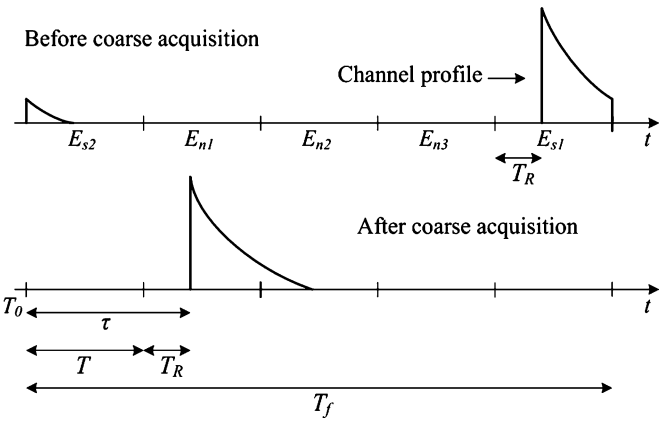


Fig. 9. Coarse acquisition step.

which is a uniformly distributed RV in $[0, T]$. By imposing $K \ge 3$, we can obtain coarse acquisition since the frame starts with a noise-only part shorter than $2T$. Therefore, with respect to the notation introduced in the previous section, we find $\tau_{\mathrm{MAX}} = 2T$, and the useful signal part goes to zero before the end of the frame since $T \approx \tau_{\mathrm{cds}}$. As an example, Fig. 9 shows the described coarse acquisition procedure, for $K = 5$.

The performance of this scheme is evaluated in terms of probability of *coarse acquisition* $P_{\mathrm{CA}}$, which is defined as the probability of having the energy in bins $s_1$ or $s_2$ greater than that in all the other bins. Calling $P_{s_1} = \Pr\{s_1 \text{ has the highest energy}\}$ and $P_{s_2} = \Pr\{s_2 \text{ has the highest energy}\}$ conditioned on a particular realization of $T_R$ results in $P_{\mathrm{CA}} \triangleq P_{s_1} + P_{s_2} - P_{s_1 \cap s_2} = P_{s_1} + P_{s_2}$ since the two events $\{s_1 \text{ has the highest energy}\}$ and $\{s_2 \text{ has the highest energy}\}$ are mutually exclusive. To evaluate $P_{\mathrm{CA}}$, a statistical characterization of $E_k$ is required. To this purpose, the IEEE UWB channel models [28] are difficult to analyze. For this reason, a simplified channel model composed of a single exponential decay and a dense path arrival rate is considered here. It will be shown that this assumption introduces negligible differences compared with results obtained using the IEEE models. A more convenient representation of the CIR is $h(t) = \sum_{l=0}^{L-1} h_{R,l}\delta(t - \tau_{R,l})$, where $L$ is the number of *resolvable* multipath components; $\tau_{R,l} = \tau_{R,0} + lT_B$ is the delay of the $l$th resolvable path, with $T_B = 1/B$; $h_{R,l} = |h_{R,l}| \exp(j\phi_l)$ is the amplitude of the $l$th resolvable path; and $\phi_l \in \{0, \pi\}$ with equal probability. $|h_{R,l}|$ is usually modeled as an RV (e.g., Nakagami distributed [28]); however, to simplify the analytical derivation, $|h_{R,l}|$ is assumed deterministic with $h_{R,l}^2 = h_{R,0}^2 \exp(-lT_B/\alpha_{\mathrm{ch}})$, where $\alpha_{\mathrm{ch}}$ is the channel power decay constant and $h_{R,0}^2 = 1/L_{\mathrm{TP}} \cdot (1 - \exp(-T_B/\alpha_{\mathrm{ch}}))$ for normalization, where $L_{\mathrm{TP}}$ is the total signal power path loss. In the link budget calculation, the *total* signal power fading $S_{\mathrm{TP}}$ can be included in this term. In this way, after normalizing to the total signal power, the small-scale fading in $|h_{R,l}|$ results only in a variation in the energy of $s_1$ and $s_2$ with respect to each other. However, due to the large number of multipath components, this variation is very small and therefore can be neglected in the analysis. Realistic values of $S_{\mathrm{TP}}$ for different bandwidths can be found in [27]. Under this hypothesis, the energy in $s_1$ and $s_2$ are given in (21) and (22), shown at the bottom of the page, respectively.

TABLE I
MEAN AND VARIANCE OF $E_{s_1}$, $E_{s_2}$ AND $E_{n_i}$

| | |
|---|---|
| $\mu_{s_1}$ | $N_{CA}(MN_0 + E_r(1 - \exp(-(T - T_R)/\alpha_{ch})))$ |
| $\sigma^2_{s_1}$ | $N_{CA}(2MN_0^2 + 4N_0E_r(1 - \exp(-(T - T_R)/\alpha_{ch})))$ |
| $\mu_{s_2}$ | $N_{CA}(MN_0 + E_r(\exp(-(T - T_R)/\alpha_{ch}) - \exp(-(2T - T_R)/\alpha_{ch})))$ |
| $\sigma^2_{s_2}$ | $N_{CA}(2MN_0^2 + 4N_0E_r(\exp(-(T - T_R)/\alpha_{ch}) - \exp(-(2T - T_R)/\alpha_{ch})))$ |
| $\mu_{n_0}$ | $N_{CA}MN_0$ |
| $\sigma^2_{n_0}$ | $2N_{CA}MN_0^2$ |

$T_{s_1}$ and $T_{s_2}$ are the starting times of $s_1$ and $s_2$, respectively, and $\otimes$ represents the convolution operation. The energy in the remaining $K-2$ noise-only bins is

$$E_{n_i} = \sum_{j=0}^{N_{\mathrm{CA}}-1} \int_{T_{n_i}+jT_f}^{T_{n_i}+T+jT_f} n^2(t)dt \tag{23}$$

for $i = 1 \ldots K-2$, where $T_{n_i}$ is the starting time of noise bin $n_i$.

$E_{s_1}$ and $E_{s_2}$ are noncentral chi-square distributed RVs with noncentrality parameters, i.e.,

$$\begin{aligned}\mu_{\mathrm{NC}}(E_{s_1}) &= \frac{N_{\mathrm{CA}}}{N_0} \int_0^T \left( \sum_{l=0}^{L-1} h_{R,l} w(t - lT_B - T_R) \right)^2 dt \\ &= \frac{N_{\mathrm{CA}}E_r}{N_0} \left( 1 - \exp\left( -\frac{T - T_R}{\alpha_{\mathrm{ch}}} \right) \right)\end{aligned} \tag{24}$$

$$\begin{aligned}\mu_{\mathrm{NC}}(E_{s_2}) &= \frac{N_{\mathrm{CA}}}{N_0} \int_0^T \left( \sum_{l=0}^{L-1} h_{R,l} w(t - lT_B + T - T_R) \right)^2 dt \\ &= \frac{N_{\mathrm{CA}}E_r}{N_0} \left( \exp\left( -\frac{T - T_R}{\alpha_{\mathrm{ch}}} \right) - \exp\left( -\frac{2T - T_R}{\alpha_{\mathrm{ch}}} \right) \right)\end{aligned} \tag{25}$$

when an ideal rectangular receive filter over the signal band is assumed and with $E_r = E_w/L_{\mathrm{TP}}$ being the received energy in a single pulse transmission. The $E_{n_i}$ are central chi-square distributed RVs. The mean and variance of a standard noncentral chi-square RV are given by $M + \mu_{\mathrm{NC}}$ and $2M + 4\mu_{\mathrm{NC}}$, respectively, where $M = 2BT + 1$ is the degrees of freedom of the signal in each bin. In this way, using (24) and (25), it is possible to directly calculate $\mu_{s_1}$, $\sigma_{s_1}$, $\mu_{s_2}$, $\sigma_{s_2}$, and $\mu_{n_0}$, $\sigma_{n_0}$, which are the mean and standard deviations of $E_{s_1}$, $E_{s_2}$, and $E_{n_i}$, respectively. For central chi-square RVs, the same expressions hold with $\mu_{\mathrm{NC}} = 0$. These parameters are reported in Table I. Since the $M$ of interest is $M \geq 100$, as will be shown in the following, $E_{s_1}$, $E_{s_2}$, and $E_{n_i}$ can be approximated as Gaussian RVs [29], where the approximation improves with increasing $N_{\mathrm{CA}}$. Now, the expressions for $P_{s_1}$ and $P_{s_2}$ become

$$\begin{aligned}P_{s_1} &= \Pr\left\{ E_{s_1} \geq \max\{E_{s_2}, E_{n_1}, \ldots, E_{n_{K-2}}\} \right\} \\ P_{s_2} &= \Pr\left\{ E_{s_2} \geq \max\{E_{s_1}, E_{n_1}, \ldots, E_{n_{K-2}}\} \right\}.\end{aligned} \tag{26}$$

Reference [30] provides an iterative solution to determine the mean and standard deviations of the maximum of a set of Gaussian RVs. However, the results are exact only for the case of two RVs. For this reason, we propose to solve the problem in two steps where we use the observation that (26) is equivalent to

$$\begin{aligned}P_{s_1} &= \Pr\left\{ E_{s_1} \geq \max\{E_{s_2}, E_{n_{\mathrm{MAX}}}\} \right\} \\ P_{s_2} &= \Pr\left\{ E_{s_2} \geq \max\{E_{s_1}, E_{n_{\mathrm{MAX}}}\} \right\}\end{aligned} \tag{27}$$

with $E_{n_{\mathrm{MAX}}} = \max\{E_{n_1}, \ldots E_{n_{K-2}}\}$. Since the bins are disjoint and $T \gg 1/B$, $E_{n_1}, \ldots E_{n_{K-2}}$ are independent and identically distributed (i.i.d.) Gaussian RVs, therefore, the pdf of $E_{n_{\mathrm{MAX}}}$ is [31]

$$\begin{aligned}f_{n_{\mathrm{MAX}}}(x) = (K-2) \left( \Phi\left( (x - \mu_{n_0})/\sigma_{n_0} \right) \right)^{K-3} \\ \cdot \phi\left( (x - \mu_{n_0})/\sigma_{n_0} \right) / \sigma_{n_0}\end{aligned} \tag{28}$$

with $\phi(x) = 1/\sqrt{2\pi} \exp(-x^2/2)$ and $\Phi(x) = \int_{-\infty}^{x} \phi(\xi) d\xi$. The mean of $E_{n_{\mathrm{MAX}}}$ is given by

$$\begin{aligned}\mu_{n_{\mathrm{MAX}}} = \int_{-\infty}^{\infty} x(K-2) \left( \Phi\left( (x - \mu_{n_0})/\sigma_{n_0} \right) \right)^{K-3} \\ \cdot \phi\left( (x - \mu_{n_0})/\sigma_{n_0} \right) / \sigma_{n_0} dx.\end{aligned} \tag{29}$$

With the change of variable $y = (x - \mu_{n_0})/\sigma_{n_0}$, results in $\mu_{n_{\mathrm{MAX}}} = \mu_{n_0} + \mu^{(0)}_{n_{\mathrm{MAX}}} \sigma_{n_0}$. In a similar way, the standard deviation of $E_{n_{\mathrm{MAX}}}$ is found as $\sigma_{n_{\mathrm{MAX}}} = \sigma^{(0)}_{n_{\mathrm{MAX}}} \sigma_{n_0}$. Here, $\mu^{(0)}_{n_{\mathrm{MAX}}}$ and $\sigma^{(0)}_{n_{\mathrm{MAX}}}$ are the mean and standard deviations of the maximum of $K-2$ i.i.d. standard Gaussian RVs. Thus, for calculating an exact expression for the mean and variance of $E_{n_{\mathrm{MAX}}}$, only a parametrization of $\mu^{(0)}_{n_{\mathrm{MAX}}}$ and $\sigma^{(0)}_{n_{\mathrm{MAX}}}$ as a function of $K-2$ is needed. Table II shows $\mu^{(0)}_{n_{\mathrm{MAX}}}$ and $\sigma^{(0)}_{n_{\mathrm{MAX}}}$ for different values of $K-2$, determined by simulation. From simulations, $E_{n_{\mathrm{MAX}}}$ can be approximated

$$E_{s_1} = \sum_{j=0}^{N_{\mathrm{CA}}-1} \int_{t=T_{s_1}+jT_f}^{T_{s_1}+T+jT_f} \left( w(t) \otimes \sum_{l=0}^{L-1} h_{R,l} \delta(t - jT_f - T_{s_1} - T_R) + n(t) \right)^2 dt \tag{21}$$

$$E_{s_2} = \sum_{j=0}^{N_{\mathrm{CA}}-1} \int_{t=T_{s_2}+jT_f}^{T_{s_2}+T+jTf} \left( w(t) \otimes \sum_{l=0}^{L-1} h_{R,l} \delta(t - jT_f - T_{s_2} - T_R) + n(t) \right)^2 dt \tag{22}$$

TABLE II
$\mu_{n_{\mathrm{MAX}}}^{(0)}$ AND $\sigma_{n_{\mathrm{MAX}}}^{(0)}$ FOR DIFFERENT VALUES OF $K-2$

| $K-2$ | 2 | 3 | 5 | 8 | 10 | 15 | 20 |
|---|---|---|---|---|---|---|---|
| $\mu_{n_{MAX}}^{(0)}$ | 0.56 | 0.85 | 1.16 | 1.42 | 1.54 | 1.74 | 1.87 |
| $\sigma_{n_{MAX}}^{(0)}$ | 0.83 | 0.75 | 0.67 | 0.61 | 0.59 | 0.55 | 0.53 |

as a Gaussian RV.[5] The last step to evaluate (27) is to determine the pdf of $E_{\mathrm{MAX1}} = \max\{E_{s_1}, E_{n_{\mathrm{MAX}}}\}$ and of $E_{\mathrm{MAX2}} = \max\{E_{s_2}, E_{n_{\mathrm{MAX}}}\}$. Based on [30], $E_{\mathrm{MAX1}}$ and $E_{\mathrm{MAX2}}$ can be approximated as Gaussian RVs; considering, for example $E_{\mathrm{MAX2}}$, the exact expressions for its mean $\mu_{\mathrm{MAX2}}$ and variance $\sigma^2_{\mathrm{MAX2}}$ are, respectively, as follows:

$$\mu_{\mathrm{MAX2}} = \mu_{s_2}\Phi(\beta_2) + \mu_{n_{\mathrm{MAX}}}\Phi(-\beta_2) + \gamma_2\phi(\beta_2) \tag{30}$$

$$\sigma^2_{\mathrm{MAX2}} = \left(\mu^2_{s_2} + \sigma^2_{s_2}\right)\Phi(\beta_2) + \left(\mu^2_{n_{\mathrm{MAX}}} + \sigma^2_{n_{\mathrm{MAX}}}\right)\Phi(-\beta_2) + (\mu_{s_2} + \mu_{n_{\mathrm{MAX}}})\gamma_2\phi(\beta_2) - \mu^2_{\mathrm{MAX2}} \tag{31}$$

where $\gamma_2 = \sqrt{\sigma^2_{s_2} + \sigma^2_{n_{\mathrm{MAX}}}}$, and $\beta_2 = (\mu_{s_2} - \mu_{n_{\mathrm{MAX}}})/\gamma_2$. Observing that, for a particular $T_R$, $E_{s_1}$ and $E_{\mathrm{MAX2}}$ are independent since the bins are disjoint and $T \gg 1/B$, we find

$$P_{s_1} = 1 - \Phi\left((\mu_{s_1} - \mu_{\mathrm{MAX2}})/\sqrt{\sigma^2_{s_1} + \sigma^2_{\mathrm{MAX2}}}\right). \tag{32}$$

In a similar way, the expression for $P_{s_2}$, which is specular, can be derived. Using (32), the final $P_{\mathrm{CA}}$ can be calculated by averaging over $T_R$ as follows:

$$P_{\mathrm{CA}} = \frac{1}{T}\int_{T_R=0}^{T}(P_{s_1} + P_{s_2})dT_R. \tag{33}$$

To obtain the presented results, $T \approx \tau_{\mathrm{cds}}$ has been assumed. However, $\tau_{\mathrm{cds}}$ is an environment- and location-dependent channel parameter, and in a real system, it is not *a priori* known. On the other hand, its exact knowledge is not required. In fact, every $T \geq \tau_{\mathrm{cds}}$ satisfies the proposed approach. A choice of $T \leq \tau_{\mathrm{cds}}$, while attractive since it allows reduction of the noise variance in each bin, needs more attention since it could lead to a wrong coarse acquisition. Due to the typically clustered nature of indoor UWB multipaths and to the fact that, if $T$ is not large enough, the maximum energy bin could differ from $s_1$ or $s_2$, even in noiseless conditions. Through simulations, we found that a choice of $T \geq 4\mu_{T_{\mathrm{med}}}$ is large enough for our purpose, where $\mu_{T_{\mathrm{med}}}$ is the expected value of the channel mean excess delay $T_{\mathrm{med}}$. $\mu_{T_{\mathrm{med}}}$ is a large-scale parameter that can be *a priori* (approximately) known. Using the IEEE CM1 $\div$ CM4 (residential and office environment), results in $\mu_{T_{\mathrm{med}}}$ between about 9 (for CM3) and 20 ns (for CM2). A value of $T$ that satisfies the previously introduced requirement is $T = 80$ ns. For the simulations, the frame period is chosen $T_f = 800$ ns (and accordingly $K = 10$). In this, the condition that allows avoidance of interframe interference $\tau_{\mathrm{cds}} \leq T_f - \max\{\tau\} = T_f - \tau_{\mathrm{MAX}} = T_f - 2T = 640$ ns is always satisfied for the considered channels. To calculate $P_{\mathrm{CA}}$, knowledge of $\alpha_{\mathrm{ch}} = T_{\mathrm{med}}$, which holds for an exponentially decaying channel response, is required. In Fig. 10, results are plotted and obtained for CM3 (LOS office environment), considering a log-normal distribution for the mean excess delay [32] and considering it deterministic and equal to its mean $\mu_{T_{\mathrm{med}}}$. The SNR at the receiver is defined as $\mathrm{SNR} = 10\log_{10} E_r/N_0$. The proposed analytical derivation is in good agreement with simulations using the IEEE models. Due to the long simulation times required, only results for $N_{\mathrm{CA}} = 1$ and $N_{\mathrm{CA}} = 10$ are shown. No significant difference arises between curves obtained from the model using the complete distribution of $T_{\mathrm{med}}$ or only its mean value. Thus, to correctly evaluate $P_{\mathrm{CA}}$, the only channel parameter required is $\mu_{T_{\mathrm{med}}}$. Moreover, since its dependence is weak, only a coarse estimate of $\mu_{T_{\mathrm{med}}}$ is needed. In Fig. 10, it is possible to choose a proper value of $N_{\mathrm{CA}}$, given the available SNR and the required $P_{\mathrm{CA}}$.

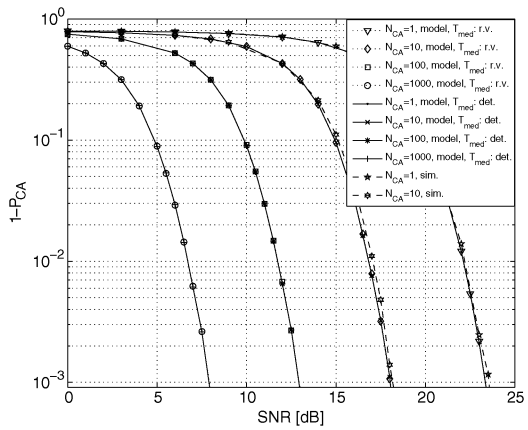


Fig. 10. Performance of proposed coarse acquisition scheme for CM3.

## VI. LINK BUDGET EVALUATION

As previously observed, the proposed TOA estimation scheme does not allow an increase of the FPNR by averaging *before* TOA estimation. This limits the maximum achievable distance. Here, the link budget provided by the presented solution is evaluated under the realistic assumption that the transmitted signal satisfies the requirements imposed by the FCC. In [22], the FCC specifies UWB emission limits in terms of EIRP peak and average power. The peak transmitted power should be less than 0 dBm when measured with a spectrum analyzer in any 50 MHz of the signal bandwidth, and the average transmitted power spectral density should be less than $-41.3$ dBm/MHz when measured in any 1 MHz of the signal bandwidth. Both requirements affect the maximum effective power $P_T^{\mathrm{MAX}}$, which can be transmitted during a single pulse. If $T_f = 800$ ns, $1/T_f = 1.25$ MHz is much smaller than the 50-MHz resolution bandwidth used for the peak power measurement compliance. Thus, from [33], the requirement on peak power gives $P_T^{\mathrm{MAX}} \leq 0.001 \cdot (B/(50 \cdot 10^6))^2$ W $\approx 35.6$ dBm. For the average power requirement, a lower bound on $P_T^{\mathrm{MAX}}$ can be determined by taking the asymptotic condition in which the pulse repetition frequency is much higher than the 1-MHz resolution bandwidth used for average power measurement compliance. This gives

[5]Note that, for $K-2 \to \infty$, it becomes an extreme value distribution; however, for $K-2 \approx 10$ or smaller, which is the case of interest here, a Gaussian approximation provides accurate results.

$P_T^{\mathrm{MAX}} \leq 7.5 \cdot 10^{-8}(BT_f)^2$ W $\approx 26.4$ dBm [33]. The received noise power in a 3-GHz bandwidth is $P_N = -174$ dBm/Hz $+ 10\log_{10}(3 \cdot 10^9) \approx -79.2$ dBm. The link margin can now be calculated considering $P_T^{\mathrm{MAX}} \approx 26.4$ dBm and a minimum $\mathrm{FPNR}_{\mathrm{MIN}} = 10$ dB, and observing that the first-peak path loss exponent $n_{\mathrm{FP}}$ is approximately 2 in LOS propagation [27]. From the relation $L_{\mathrm{FP}} = -10\log_{10}((c/(4\pi f_0 d))^{n_{\mathrm{FP}}}) \leq P_T^{\mathrm{MAX}} - P_N - FPNR_{\mathrm{MIN}}$, results in $d_{\mathrm{MAX}} \approx 300$ m.

It is worth noting that while the fine TOA estimation is based on the first peak, which propagates with path loss exponent $n_{\mathrm{FP}}$, the coarse acquisition step is based on the total signal, which propagates with path loss exponent $n_{\mathrm{TP}}$. Realistic values of $n_{\mathrm{TP}}$ can be found in [27] and [28]. With similar motivations as those previously described, by imposing a maximum achievable distance of $d_{\mathrm{MAX}} \approx 300$ m, the minimum $N_{\mathrm{CA}}$ required by the coarse acquisition step can be determined. The minimum SNR required to reach $d_{\mathrm{MAX}}$ is $\mathrm{SNR}_{d_{\mathrm{MAX}}} = P_T^{\mathrm{MAX}} - P_N - L_{\mathrm{TP}}$, where $L_{\mathrm{TP}} = -10\log_{10}((c/(4\pi f_0 d_0))^2 (d_0/d_{\mathrm{MAX}})^{n_{\mathrm{TP}}})$. Considering that, for the IEEE models, the worst case value (for LOS propagation) of $n_{\mathrm{TP}} = 1.79$ for CM3, this results in a $\mathrm{SNR}_{d_{\mathrm{MAX}}} \approx 15.6$ dB. From this value, we can calculate the minimum $N_{\mathrm{CA}}$ needed to achieve the target $P_{\mathrm{CA}}$ with the plots in Fig. 10. For example, if $1 - P_{\mathrm{CA}} \leq 10^{-3}$, $N_{\mathrm{CA}} \approx 40$ is required. The curves in Fig. 10 have been derived without considering fading in the total received power. This can be accounted for by using a fading margin of a few decibels in the link budget analysis for the total power. In a similar way, the link margin for NLOS propagation can be evaluated. The main difference in this case is the reduced coverage, which is strongly dependent on the environment. For example, when using the channel parameters as reported in [27], the maximum achievable distance in NLOS is reduced by a factor of about 5.

The suggested set of system parameters appears a reasonable choice for short-to-medium range indoor positioning applications; however, the achieved maximum distance is not a strict limit, and significantly larger distances are possible with a different choice of the parameters of interest: $N$, $N_{\mathrm{TH}}$, and the required FPNR.

## VII. Conclusion

In this paper, a low-complexity receiver for TOA estimation using UWB impulse signals has been proposed, and its performance has been evaluated. The receiver concept, which is based on two peak detectors combined with a first-order time-decay $RC$ network, requires a limited amount of processing to estimate the TOA of the received signal. It is shown that, with a 50-MHz sampling rate, the specific receiver-related errors can be neglected, and the final range estimation accuracy is at centimeter level. Since the proposed receiver directly estimates the TOA from the instantaneous received signal, it does not allow to increase the effective SNR by signal averaging *before* TOA estimation. A statistical framework is presented to enhance the accuracy of the estimated TOA by processing multiple TOA estimates from individually transmitted pulse signals. For a given required estimation accuracy value, which is determined by the probabilities of EFA and MD, a tradeoff can be made between the SNR, the required number of received pulses above a preset threshold, and the number of pulses that has to be processed. This analysis was verified using simulations based on actual measured UWB CIRs. The statistical framework has been extended to evaluate impairments due to NBI based on the first threshold crossing probability for Gaussian noise with time-varying boundaries. Finally, a coarse acquisition scheme based on maximum energy detection is described. This step is required for proper operation of the proposed TOA estimation receiver. The analytical performance of the approach is derived and compared with simulations using IEEE models. It is shown that the only relevant channel parameter that affects the coarse acquisition performance is the expected value of the channel's mean excess delay. Based on the FCC power limitations for UWB signals, a link budget analysis shows that reliable ranging is feasible up to 300 m in LOS situations and up to 60 m in NLOS cases. The proposed TOA estimation technique avoids the main technological challenges, which make it difficult to practically implement high-accuracy UWB positioning systems, namely the high sampling rates and the related complex signal processing at the receiver. For this reason, it is particularly suited for indoor positioning applications, which have strict requirements on cost and complexity.

## References


[1] M. Z. Win and R. A. Scholtz, "Ultra-wide bandwidth time-hopping spread-spectrum impulse radio for wireless multiple-access communications," *IEEE Trans. Commun.*, vol. 48, no. 4, pp. 679–689, Apr. 2000.

[2] L. Yang and G. B. Giannakis, "Ultra-wideband communications: An idea whose time has come," *IEEE Signal Process. Mag.*, vol. 21, no. 6, pp. 26–54, Nov. 2004.

[3] A. F. Molisch, "Ultrawideband propagation channels-theory, measurements, and modeling," *IEEE Trans. Veh. Technol.*, vol. 54, no. 5, pp. 1528–1545, Sep. 2005.

[4] S. Gezici, Z. Tian, G. B. Giannakis, H. Kobayashi, A. F. Molisch, H. V. Poor, and Z. Sahinoglu, "Localization via ultra-wideband radios: A look at positioning aspects for future sensor networks," *IEEE Signal Process. Mag.*, vol. 22, no. 4, pp. 70–84, Jul. 2005.

[5] G. Bellusci, G. J. M. Janssen, J. Yan, and C. C. J. M. Tiberius, "Model of the distance and bandwidth dependency of TOA-based UWB ranging error," in *Proc. IEEE ICUWB*, Sep. 2008, pp. 193–196.

[6] D. Dardari, A. Conti, U. Ferner, A. Giorgetti, and M. Z. Win, "Ranging with ultrawide bandwidth signals in multipath environments," *Proc. IEEE*, vol. 97, no. 2, pp. 404–426, Feb. 2009.

[7] Z. N. Low, J. H. Cheong, C. L. Law, W. T. Ng, and F. Watanabe, "Pulse detection algorithm for line-of-sight (LOS) UWB ranging applications," in *Proc. IEEE Antennas Wireless Propag. Lett.*, 2005, vol. 4, pp. 63–67.

[8] C. Mazzucco, U. Spagnolini, and G. Mulas, "A ranging technique for UWB indoor channel based on power delay profile analysis," in *Proc. IEEE VTC*, May 2004, vol. 5, pp. 2595–2599.

[9] J.-Y. Lee and R. A. Scholtz, "Ranging in a dense multipath environment using an UWB radio link," *IEEE J. Sel. Areas Commun.*, vol. 20, no. 9, pp. 1677–1683, Dec. 2002.

[10] A. A. D'Amico, U. Mengali, and L. Taponecco, "Energy-based TOA estimation," *IEEE Trans. Wireless Commun.*, vol. 7, no. 3, pp. 838–847, Mar. 2008.

[11] I. Guvenc and Z. Sahinoglu, "Threshold-based TOA estimation for impulse radio UWB systems," in *Proc. IEEE ICU*, Sep. 2005, pp. 420–425.

[12] M. Chiani and A. Giorgetti, "Coexistence between UWB and narrow-band wireless communication systems," *Proc. IEEE*, vol. 97, no. 2, pp. 231–254, Feb. 2009.

[13] A. Giorgetti, M. Chiani, and M. Z. Win, "The effects of narrowband interference on wideband wireless communication systems," *IEEE Trans. Commun.*, vol. 53, no. 12, pp. 2139–2149, Dec. 2005.

[14] A. Rabbachin, T. Q. S. Quek, P. C. Pinto, I. Oppermann, and M. Z. Win, "UWB energy detection in the presence of multiple narrowband interferers," in *Proc. IEEE ICUWB*, Sep. 24–26, 2007, pp. 857–862.

[15] T. Q. S. Quek, M. Z. Win, and D. Dardari, "Unified analysis of UWB transmitted reference schemes in the presence of narrowband interference," *IEEE Trans. Wireless Commun.*, vol. 6, no. 6, pp. 2126–2139, Jun. 2007.
[16] D. Dardari, A. Conti, U. Ferner, A. Giorgetti, and M. Z. Win, "Time-of-arrival estimation of UWB signals in the presence of narrowband and wideband interference," in *Proc. IEEE ICUWB*, Sep. 2007, pp. 71–76.
[17] L. M. Ricciardi and S. Sato, "On the evaluation of first-passage-time densities for Gaussian processes," *Signal Process.*, vol. 11, no. 4, pp. 339–357, Dec. 1986.
[18] E. di Nardo, A. G. Nobile, E. Pirozzi, and L. M. Ricciardi, "On the asymptotic behavior of first passage time densities for stationary Gaussian processes and varying boundaries," *Methodol. Comput. Appl. Probability*, vol. 5, no. 2, pp. 211–233, Jun. 2003.
[19] C. Carbonelli and U. Mengali, "Synchronization algorithms for UWB signals," *IEEE Trans. Wireless Commun.*, vol. 7, no. 3, pp. 838–847, Mar. 2008.
[20] A. Rabbachin and I. Oppermann, "Synchronization analysis for UWB systems with a low-complexity energy collection receiver," in *Proc. Joint UWBST/IWUWBS*, May 2004, pp. 288–292.
[21] S. Gezici, Z. Sahinoglu, A. F. Molisch, H. Kobayashi, and H. V. Poor, "Two-Step Time of Arrival Estimation for Pulse Based Ultra-Wideband Systems," in *Proc. EURASIP JASP*, 2008.
[22] "Revision of part 15 of the commission's rules regarding ultra-wideband transmission systems," FCC, Washington, DC, ET Docket 98-153, 2002.
[23] P. H. Young, *Electronic Communication Techniques*, 5th ed. Englewood Cliffs, NJ: Prentice-Hall, 2004.
[24] I. F. Blake, W. C. Lindsey, and F. Watanabe, "Level crossing problems for random processes," *IEEE Trans. Inf. Theory*, vol. IT-19, no. 3, pp. 295–315, May 1973.
[25] J.-Y. Lee and S. Yoo, "Large error performance of UWB ranging in multipath and multiuser environments," *IEEE Trans. Microw. Theory Tech.*, vol. 54, no. 4, pp. 1887–1895, Apr. 2006.
[26] G. Bellusci, G. J. M. Janssen, J. Yan, and C. C. J. M. Tiberius, "A low-complexity UWB receiver concept for TOA based indoor ranging," in *Proc. IEEE ICUWB*, Sep. 2009, pp. 618–623.
[27] G. Bellusci, G. J. M. Janssen, J. Yan, and C. C. J. M. Tiberius, "Low-complexity UWB ranging in indoor multipath environments," in *Proc. IEEE-ION*, May 2008, pp. 394–401.
[28] A. F. Molisch, D. Cassioli, C. C. Chong, S. Emami, A. Fort, B. Kannan, J. Karedal, J. Kunisch, H. G. Schantz, K. Siwiak, and M. Z. Win, "A comprehensive standardized model for ultrawideband propagation channels," *IEEE Trans. Antennas Propag.*, vol. 54, no. 11, pp. 3151–3166, Nov. 2006.
[29] P. A. Humblet and M. Azizoglu, "On the bit error rate of lightwave systems with optical amplifiers," *J. Lightw. Technol.*, vol. 9, no. 11, pp. 1576–1582, Nov. 1991.
[30] C. E. Clark, "The greatest of a finite set of random variables," *Oper. Res.*, vol. 9, no. 2, pp. 145–162, Mar./Apr. 1961.
[31] A. Balakrishnan and A. Cohen, *Order Statistics and Inference—Estimation Methods*. New York: Academic, 1990.
[32] I. Guvenc, C. C. Chong, and F. Watanabe, "NLOS identification and mitigation techniques for UWB localization systems," in *Proc. IEEE WCNC*, Mar. 2007, pp. 1571–1576.
[33] R. J. Fontana and E. A. Richley, "Observations on Low Data Rate, Short Pulse UWB Systems," in *Proc. IEEE ICUWB*, Sep. 2007, pp. 334–338.

**Giovanni Bellusci** received the B.Sc. and M.Sc. degrees in telecommunication engineering (both *cum laude*) from the University of Pisa, Pisa, Italy, in 2003 and 2005, respectively, and the Ph.D. degree from the Delft University of Technology, Delft, The Netherlands, in 2011.

Since 2010, he has been with Xsens Technologies B.V., Enschede, The Netherlands. His research interests include ultrawideband radio, communication theory, statistical signal processing, wireless sensor networks, positioning, tracking, and sensor fusion algorithms.

**Gerard J. M. Janssen** received the M.Sc.E.E. degree from Eindhoven University of Technology, Eindhoven, The Netherlands, in 1986 and the Ph.D. degree from Delft University of Technology, Delft, The Netherlands, in 1998.

He is currently an Associate Professor with the Circuits and Systems Group, Delft University of Technology. His research interests include wireless communication, particularly narrowband multiuser detection, digital modulation techniques, channel modeling, diversity techniques, and ultrawideband communications and positioning.

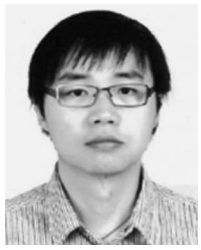

**Junlin Yan** received the M.Sc. degree in digital communications from Chalmers University of Technology, Sweden, in 2006 and the Ph.D. degree in algorithms for indoor positioning systems from Delft University of Technology, Delft, The Netherlands, in 2010.

He is currently a System Engineer with Intel Mobile Communications GmbH, Duisburg, Germany. His research interests include navigation, particularly in Global Navigation Satellite Systems and indoor positioning.

**Christian C. J. M. Tiberius** received the Ph.D. degree in recursive data processing for kinematic GPS surveying from the Delft University of Technology, Delft, The Netherlands, in 1998.

He is currently an Associate Professor with the Department of Geoscience and Remote Sensing, Delft University of Technology. He is and has been responsible for many projects in the area of navigation with national and international agencies, such as the European Space Agency and industry as well. His research interest include navigation, primarily with Global Navigation Satellite Systems and indoor radio positioning.